Supplementary Information
The Effect of Molecular Shape and Pore Structure on Local and Nanoscale Cresol Behaviour in Commercial Zeolite Catalysts

K. S. C. Morton, A. J. Porter, J. Armstrong, and A. J. O'Malley

S1 Constructing molecular dynamics simulations

The unit cell parameters of the zeolite frameworks H-Y, H-Beta and H-ZSM5 after equilibration at constant pressure are a factor of 1.01–1.03 times larger than experimental values[1], shown in table S1.

Table S1: The unit cell parameters of the zeolite frameworks H-Y, H-Beta and H-ZSM5 after equilibration at constant pressure, compared with experimental values.

	Simulated unit cell parameters (Å)			**Experimental unit cell parameters (Å)**		
Zeolite Type	**a**	**b**	**c**	**a**	**b**	**c**
H-Y	24.8239	24.8239	24.8239	24.3540	24.3540	24.3540
H-Beta	12.7929	12.7929	26.5196	12.6320	12.6320	26.1860
H-ZSM5	20.6779	20.3156	13.5266	20.0900	19.7380	13.1420

Table S2: Potential parameters describing inter-atomic zeolite interactions.
*Denotes Si/Al atoms.

Buckingham, $U(r_{ij}) = A \times e^{(-\frac{r_{ij}}{\rho})} - \frac{C}{r_{ij}^6}$			
Atoms	A (eV)	ρ (Å)	C (eV Å^6)
O^{2-} O^{2-}	22764.0000	0.14900	27.8800
O^{2-} $O^{1.426-}$	22764.0000	0.14900	27.8800
O^{2-} $H^{1.426+}$	311.9700	0.25000	0.0000
O^{2-} Si^{4+}	1283.9070	0.32052	10.66158
O^{2-} Al^{3+}	1460.3000	0.29912	0.00000
$O^{1.426-}$ Si^{4+}	983.5566	0.32052	10.66158
$O^{1.426-}$ Al^{3+}	1142.6775	0.29912	0.00000
Morse, $U(r_{ij}) = D_0 \left(\left(1 - e^{-k(r_{ij} - r_0)}\right)^2 - 1 \right)$			
Atoms	D_0 (eV)	r_0 (Å)	k (Å^{-1})
$O^{1.426-}$ $H^{1.426+}$	7.0525	0.9485	2.1986
Three body harmonic, $U(\theta_{ijk}) = \frac{k}{2}(\theta_{ijk} - \theta_0)^2$			
Atoms	k (eV rad^{-2})	θ_0 (°)	Cut-off (Å)
O...T*...O	2.09724	109.47	2.5

Table S3: Potential parameters describing cresol intramolecular forces.
*SF are the 1-4 interaction scale factors.

Harmonic bond, $U(r_{ij}) = \frac{k}{2}(r_{ij} - r_0)^2$					
Bond	k ($\mathrm{eV^{-1}\ \AA^{-2}}$)			r_0 (Å)	
H-O	47.96			0.945	
O-C_a	39.03			1.364	
C_a-C_a	40.68			1.400	
C_a-H_a	31.83			1.080	
C_a-C_t	27.49			1.510	
C_t-H_t	29.49			1.090	
Harmonic bond angle, $U(\theta_{ijk}) = \frac{k}{2}(\theta_{ijk} - \theta_0)^2$					
Angle	k ($\mathrm{eV^{-1}\ rad^{-2}}$)			θ_0 (°)	
H-O-C_a	3.035490			113.0	
O/C_t-C_a-C_a	6.070981			120.0	
C_a-C_a-C_a	5.463883			120.0	
C_a-C_a-H_a	3.035490			120.0	
C_a-C_t-H_t	3.035490			109.5	
H_t-C_t-H_t	2.862034			107.8	
Triple cosine dihedral, $U(\phi_{ijkl}) = \frac{1}{2}\left(A_1(1+\cos(\phi_{ijkl})) + A_2(1-\cos(2\phi_{ijkl})) + A_3(1+\cos(3\phi_{ijkl}))\right)$					
Dihedral	A_1 ($\mathrm{eV^{-1}}$)	A_2 ($\mathrm{eV^{-1}}$)	A_3 ($\mathrm{eV^{-1}}$)	Electrostatic SF*	Van der Waals SF*
H-O-C_a-C_a	0.0	0.072939	0.0	0.5	0.5
H_a/C_a-C_a-C_a-C_a/H_a/C_t/O	0.0	0.314390	0.0	0.0	0.0
C_a-C_a-C_t-H_t	0.0	0.000000	0.0	0.5	0.5
For *p*-cresol:					
C_t-C_{a4}-C_{a3}-C_{a5}, O-C_{a6}-C_{a1}-C_{a2}	0.0	0.346913	0.0	0.0	0.0
C_{a4}-C_{a6}-C_{a5}-H_{a5}, C_{a4}-C_{a2}-C_{a3}-H_{a3}, C_{a5}-C_{a1}-C_{a6}-H_{a6}, C_{a3}-C_{a1}-C_{a2}-H_{a2}	0.0	0.095401	0.0	0.0	0.0
For *m*-cresol:					
C_t-C_{a5}-C_{a4}-C_{a6}, O-C_{a6}-C_{a1}-C_{a2}	0.0	0.346913	0.0	0.0	0.0
C_{a5}-C_{a1}-C_{a6}-H_{a6}, C_{a5}-C_{a3}-C_{a4}-H_{a4}, C_{a4}-C_{a2}-C_{a3}-H_{a3}, C_{a1}-C_{a3}-C_{a2}-H_{a2}	0.0	0.095401	0.0	0.0	0.0

Table S4: Potential parameters describing cresol intermolecular forces and atom charges.

Lennard-Jones, $U(r_{ij}) = 4\epsilon_{ij}\left(\frac{\theta_{ij}}{r_{ij}}^{12} - \frac{\theta_{ij}}{r_{ij}}^{6}\right),\ \epsilon_{ij} = (\epsilon_i \times \epsilon_j)^{\frac{1}{2}},\ \theta_{ij} = \frac{1}{2}(\theta_i + \theta_j)$				
Atom	p-cresol: q (e^-)	m-cresol: q (e^-)	ϵ_i (eV^{-1})	θ_i (Å)
H	0.4456	0.4461	0.001301	0.50
O	-0.5970	-0.5969	0.007372	3.07
C_{a1}	0.2025	0.2100	0.003036	3.55
C_{a2}	-0.1863	-0.2263	0.003036	3.55
C_{a6}	-0.1863	-0.1577	0.003036	3.55
C_{a3}	-0.0908	-0.0872	0.003036	3.55
C_{a5}	-0.0908	-0.0451	0.003036	3.55
C_{a4}	-0.1179	-0.1656	0.003036	3.55
C_t	-0.1220	-0.1276	0.002862	3.50
H_{a2}	0.1368	0.1284	0.001301	2.42
H_{a6}	0.1368	0.1447	0.001301	2.42
H_{a3}	0.1333	0.1310	0.001301	2.42
H_{a5}/H_{a4}	0.1333	0.1315	0.001301	2.42
H_t	0.0676	0.0715	0.001301	2.50

Table S5: Potential parameters describing zeolite-cresol interactions.
*Denotes cresol molecule atoms.

Buckingham			
Atoms	A (eV)	ρ (Å)	C (eV Å^6)
Si O*	410.8502	0.32052	10.66158
Al O*	467.2960	0.29912	0.00000
Lennard-Jones			
Atom	ϵ_i (eV^{-1})	θ_i (Å)	
O C*	0.008430	2.958	
O H*	0.004987	2.557	
O O*	0.010545	2.764	
H C*	0.003900	2.806	
H H*	0.000851	1.785	
H O*	0.000000	1.535	

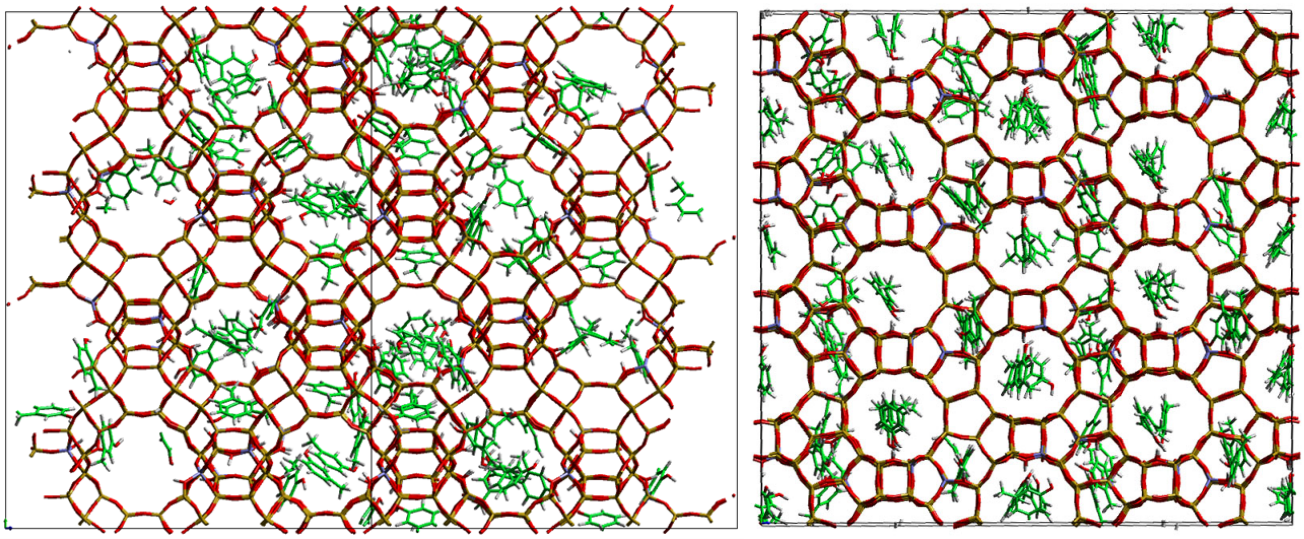

(a) (b)

Figure S1: Systems equilibrated at 370 K of 10% wt. of *m*-cresol loaded into zeolites (a) H-Y viewed along [110] and (b) H-Beta viewed along [100].

S2 Quasielastic neutron scattering

3D QENS spectra varying with Q for each sample collected at 370 K are shown in figure S2.

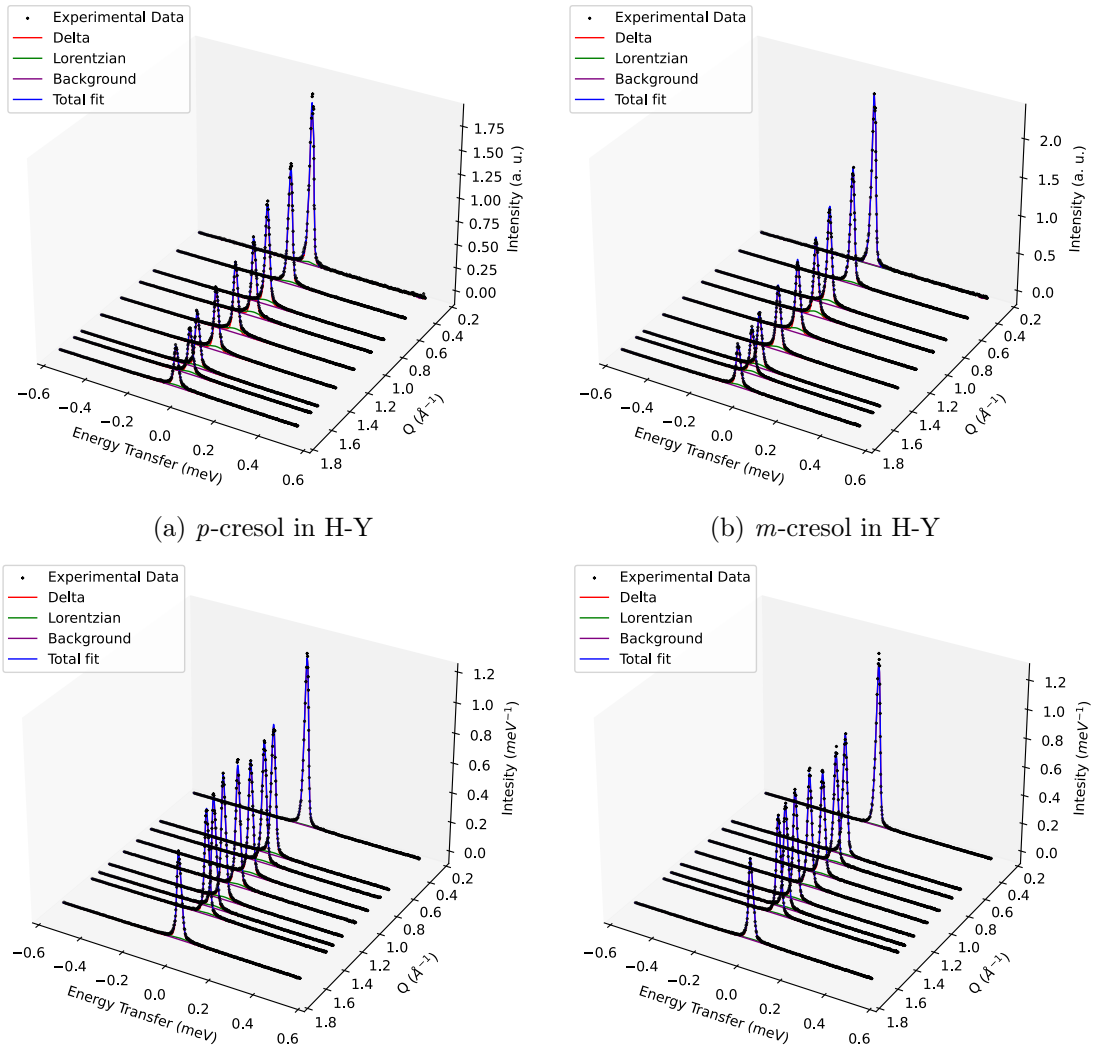

(a) p-cresol in H-Y

(b) m-cresol in H-Y

(c) p-cresol in H-Beta

(d) m-cresol in H-Beta

Figure S2: 3D QENS spectra of p-cresol and m-cresol in H-Y and H-Beta at 370 K.

2D QENS spectra for each sample measured at 370 K and at Q ~0.95 Å^{-1} are shown in figure S3, each fit by a convolution of a delta function, a flat background and a single Lorentzian function.

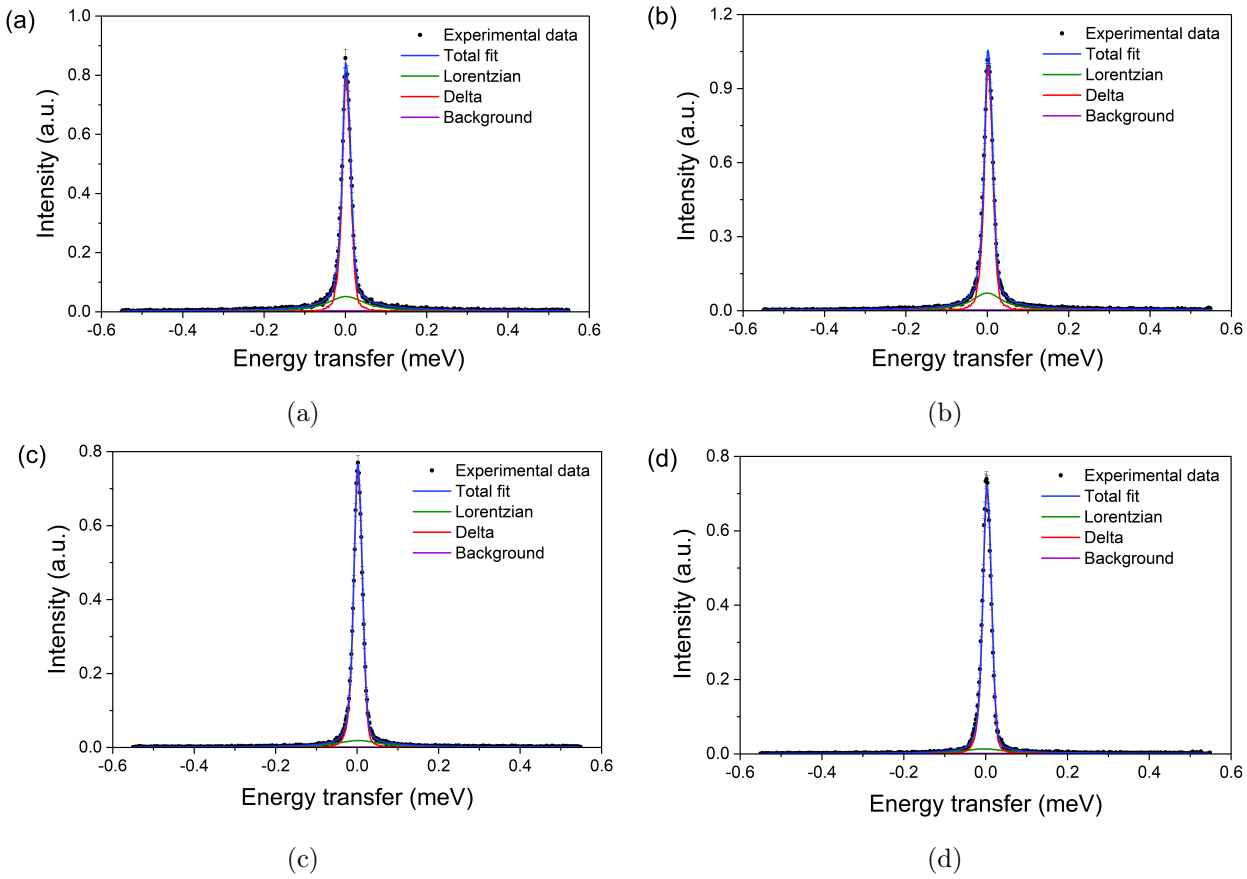

Figure S3: QENS spectra of (a) *p*-cresol and (b) *m*-cresol in H-Y, (c) *p*-cresol and (d) *m*-cresol in H-Beta at 370 K and Q ~0.95 Å^{-1}.

The mobility of a system and the types of motions occurring within it can be analysed by fitting models to the elastic incoherent structure factor (EISF) as a function of momentum transfer, Q. The validity of different types of motions can be confirmed by fittings models to the half-width half-maxima (HWHM) of the Lorentzian functions as a function of Q, from which the rates of the motions can be determined.

Many models are available to describe the local and long-range dynamics of small molecules. Long-range, unconfined translation is characterised by a Lorentzian HWHM that can be fit by a model that increases with Q^2 and passes through the origin. As a consequence of the QENS experiments probing short timescales, only a single, broad Lorentzian function was required to fit the data. The HWHM of the Lorentzian did not exhibit a relationship with Q^2, and hence models for translation were not considered. A number of models describing localised dynamics were considered, and are discussed in detail below.

S2.1 Modelling different modes of motion

A cresol molecule confined to a spherical volume such as a zeolite pore, as seen in figure 3(a) in the main text, can be described by the Volino-Dianoux model of confined diffusion[2]. Confined diffusion is indicated by a fixed Lorentzian HWHM ($\Delta\omega(Q)$) at low Q^2 corresponding to a lack of movement over long distances, and an increasing HWHM at high Q^2 corresponding to translation over shorter distances within a confined volume with a radius of r_{conf}.

The EISF for confined diffusion is depicted below.

$$EISF = \left(\frac{3j_1(Qr_{conf})}{Qr_{conf}}\right)^2 \tag{1}$$

Isotropic rotation, modelled by Sears[3], describes a molecule's random re-orientation around any axis, as depicted in figure 3(b) in the main text. The HWHM of the Lorentzians corresponding to rotational motions show no trend with Q^2. The rate of isotropic rotation is calculated from the average of the HWHM values. Its EISF is defined below.

$$EISF = j_0^2(Qr) \tag{2}$$

Where j_n is the n^{th} spherical Bessel function and r is the radius of rotation.

A molecule or substituent rotating around a single axis, can be described through the use of a model employing N number of jumps around a fixed axis, with a radius of r, shown in figures 3(c) and (d) in the main text. This can be a 'continuous' rotation where N is large or the rotating group can have a fixed number of minimal energy positions that it jumps between. This model assumes that any protons not involved in the rotation are immobile and so the EISF is scaled by $\frac{H_r}{H_t}$, where H_r and H_t are the rotating and total numbers of hydrogens respectively.

A 3-site rotation model ($N = 3$) can describe a rotating methyl group, where its identical protons jump between three minimal energy positions and r is the methyl group radius depicted in figure 3(c), set to the average methyl radius calculated from the simulations ($r = 1.18$ Å).

A uniaxial rotation such as a cresol molecule bonding through its hydroxy group to a zeolite BAS was also considered, where the jumping was approximated as continuous ($N > 40$) and the radius was equivalent to that of the rotating protons (any protons aligned with the axis were considered immobile). This is shown in figure 3(d).

$$EISF = \frac{H_r}{H_t}\left(\frac{1}{N}\left(1 + 2j_0\left(Qr^{\frac{1}{N}}\right)\right)\right) + \left(1 - \frac{H_r}{H_t}\right) \tag{3}$$

Any one of the above models may not describe the experimental data accurately due to a degree of immobilisation of the scattering objects on the instrumental timescale. Therefore, the models can incorporate both a percentage of mobilised (p_x) and static molecules ($1 - p_x$) to give the effective EISF ($EISF_{eff}$).

$$EISF_{eff} = p_x(EISF) + (1 - p_x) \tag{4}$$

S2.2 Experimental QENS analysis

Only single models of motion were applied to fit the EISFs due to the presence of single Lorentzian. Models of the aforementioned motions fit to the experimental EISFs are shown in figure S4 for a single sample.

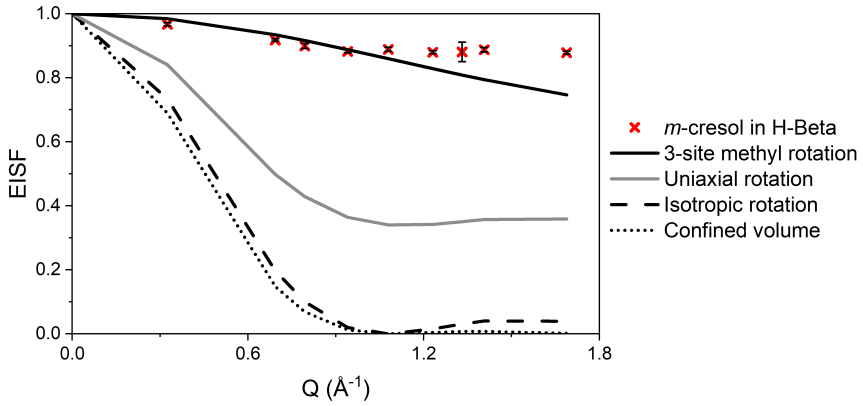

Figure S4: Experimental EISF of *m*-cresol in H-Beta at 370 K, fit by models of motion.

A better fit of the models to the data are achieved when immobile fractions of cresol molecules are introduced, shown in figure S5.

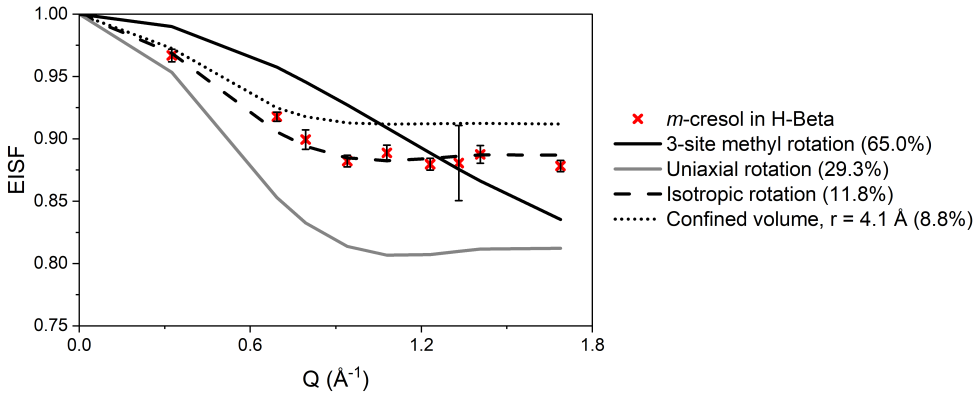

Figure S5: Experimental EISF of *m*-cresol in H-Beta at 370 K, fit by models of motion incorporating an immobile fraction. Percentages of mobile molecules are shown in brackets.

The confined diffusion, 3-site rotation and uniaxial rotation models did not provide good fits to the EISFs, especially when describing cresol behaviour in H-Beta. It is likely that any methyl rotation that occurred was on a timescale that was too fast for the instrument to measure and this may be accounted for, in part, by the flat background. It should be mentioned that a continuous methyl rotation model ($N > 40$) and a 2-site axial rotation of cresols bound to BASs ($N = 2$) were also trialled and gave even lower quality fits than the models displayed in figure S5, and so were removed for clarity.

The model that gave the best fit to each of the systems sampled at every temperature was a model of isotropic rotation, including an immobile proportion of cresol molecules in each fit, as observed in figure S6.

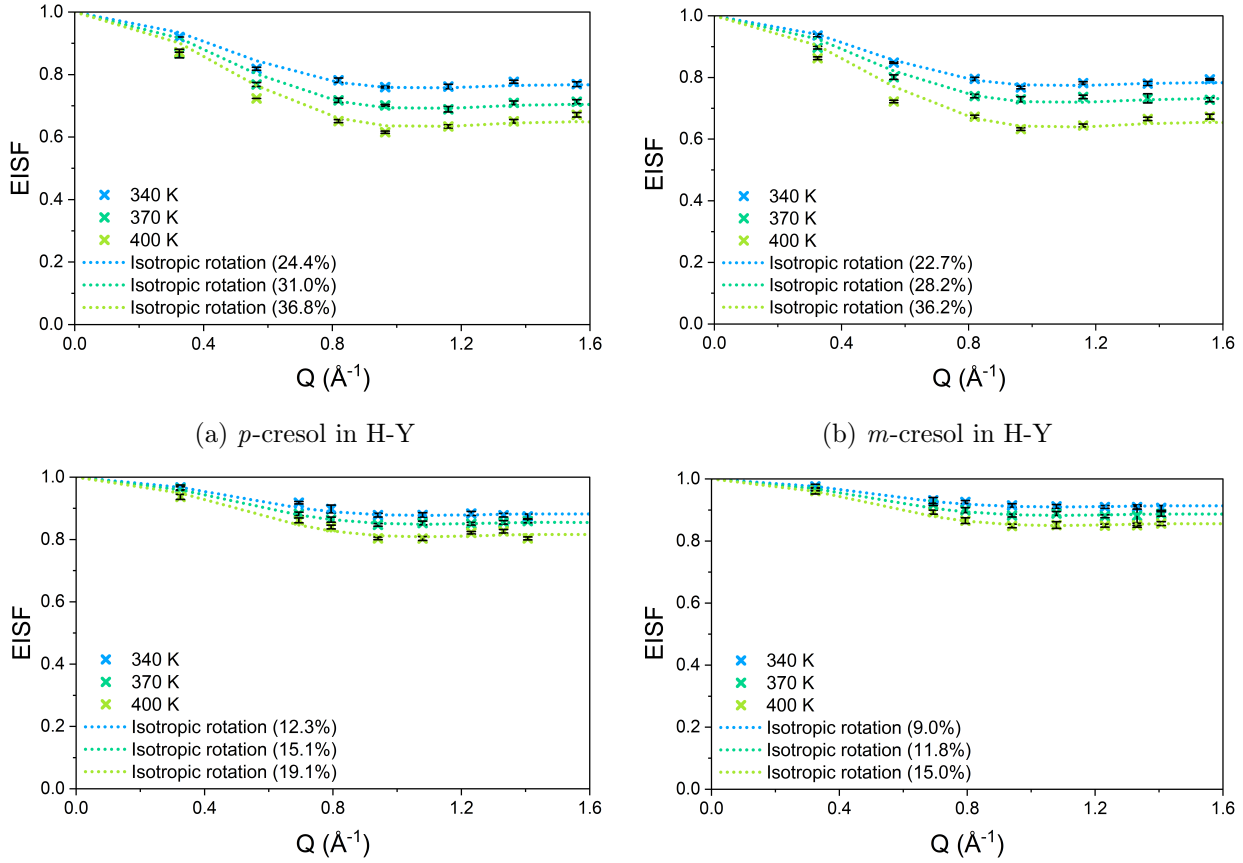

(a) *p*-cresol in H-Y

(b) *m*-cresol in H-Y

(c) *p*-cresol in H-Beta

(d) *m*-cresol in H-Beta

Figure S6: Experimental EISFs of *p*- and *m*-cresol in H-Y and H-Beta from 340–400 K, fit by models of isotropic rotation. Percentages of mobile molecules are shown in brackets.

The HWHM data sampled at 370 K are shown in figure S14 showing the trends with sample type, and every sample measured from 340–400 K are displayed in figure S8, from which the rotational coefficients were calculated.

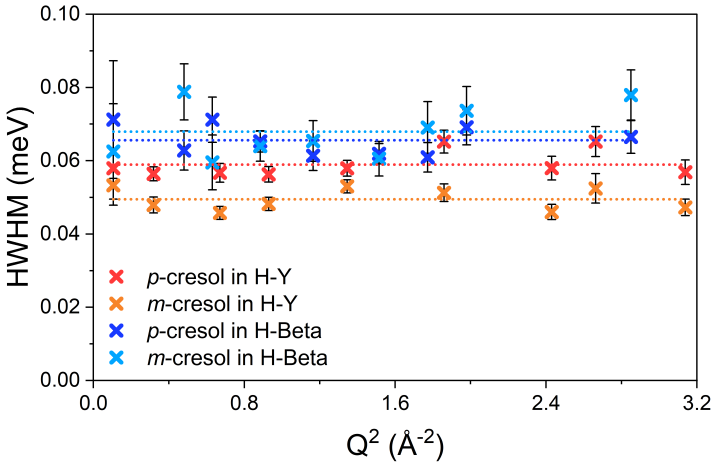

Figure S7: HWHM of the Lorentzian components of the QENS spectra for *p*- and *m*-cresol in H-Y and H-Beta at 370 K, fit by models of rotation.

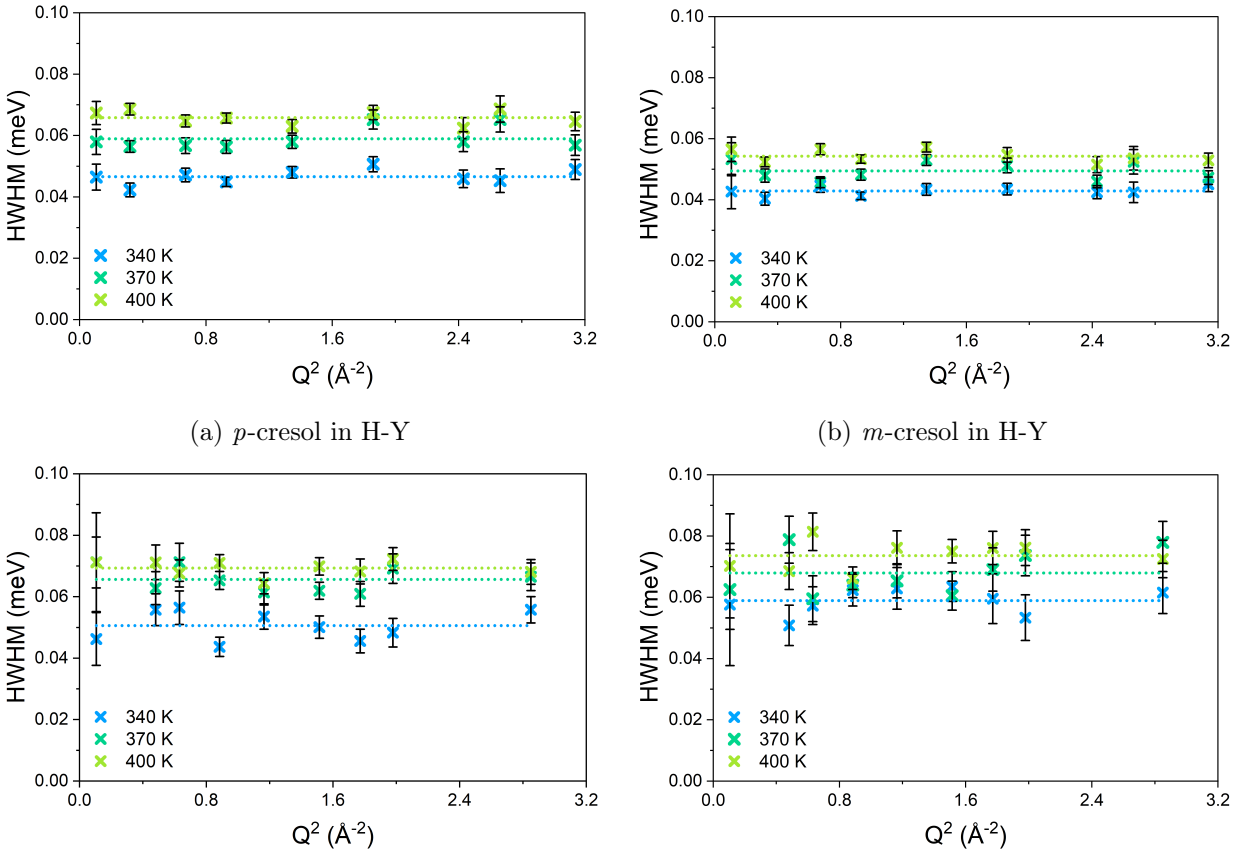

(a) *p*-cresol in H-Y

(b) *m*-cresol in H-Y

(c) *p*-cresol in H-Beta

(d) *m*-cresol in H-Beta

Figure S8: HWHM of the Lorentzian components of the QENS spectra of *p*- and *m*-cresol in H-Y and H-Beta from 340–400 K, fit by models of rotation.

The obtained rotational coefficients were then used to calculate their respective activation energies (E_a) via the Arrhenius plots shown below.

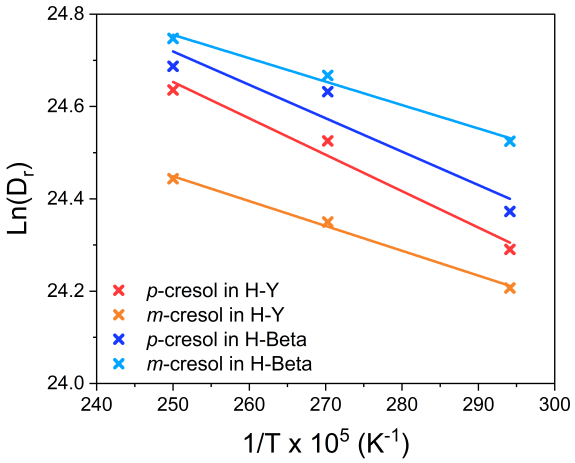

Figure S9: Arrhenius plots used to calculate the experimental E_a values for isotropic rotation.

S3 Molecular dynamics simulations

S3.1 Reproducing QENS observables and local motions

Examples of intermediate scattering functions (ISFs) obtained from the simulated systems at 370 K for $Q \sim 0.95$ Å^{-1} are shown in figure S10. The employment of two exponentials were required to obtain sufficient fits to the ISFs.

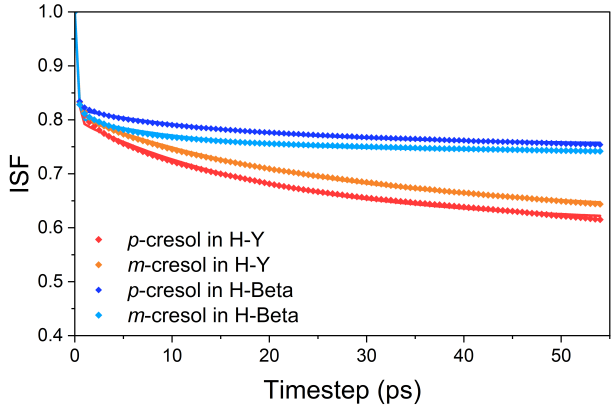

Figure S10: Rotational ISFs of *p*- and *m*-cresol in H-Y and H-Beta at 370 K and $Q \sim 0.95$ Å^{-1}, and their associated fittings.

As shown in figure S11, single models of rotational motions did not adequately fit the simulated EISFs obtained from the baselines of the ISFs, even with a proportion of immobility included.

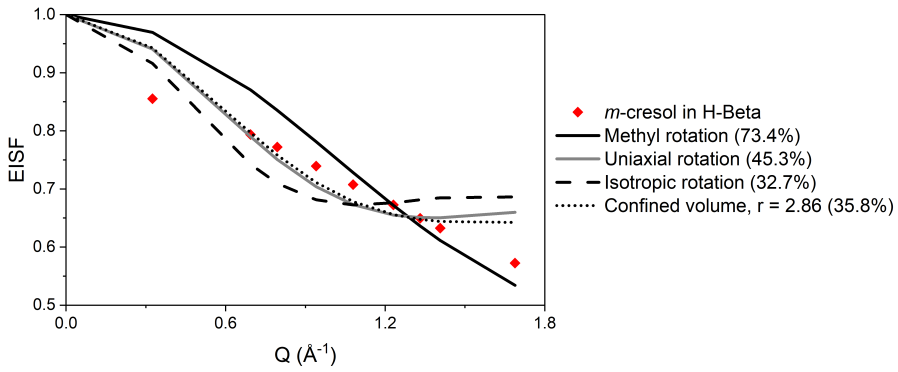

Figure S11: Simulated EISF of *m*-cresol in H-Beta at 370 K, fit by models of motion incorporating an immobile fraction. The percent of mobile molecules are shown in brackets.

Therefore, a linear combination of two rotational models were required to give good fits to the EISFs, which is expected due to the presence of two exponential functions required to fit the ISFs. The combined models of motion that gave the best fits to the data, and the respective weightings of each model, are shown in figure S12.

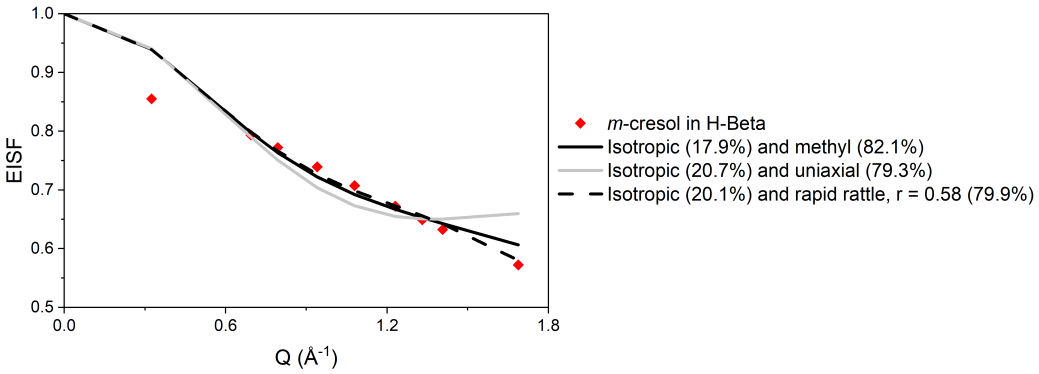

Figure S12: Simulated EISF of *m*-cresol in H-Beta at 370 K, fit by combined models of motion. The percent of each model contributing to the total model are shown in brackets.

It is clear, that for this system at least, the model combining an isotropic model with a model of rapid rattling where the radii were allowed to vary gave the best fits to the simulated EISFs, similar to the dynamics observed for phenol and catechol in H-Beta found by Hernandez-Tamargo *et al.*[4].

The fittings of this combined model to the EISFs of all systems at every temperature are displayed in figure S13.

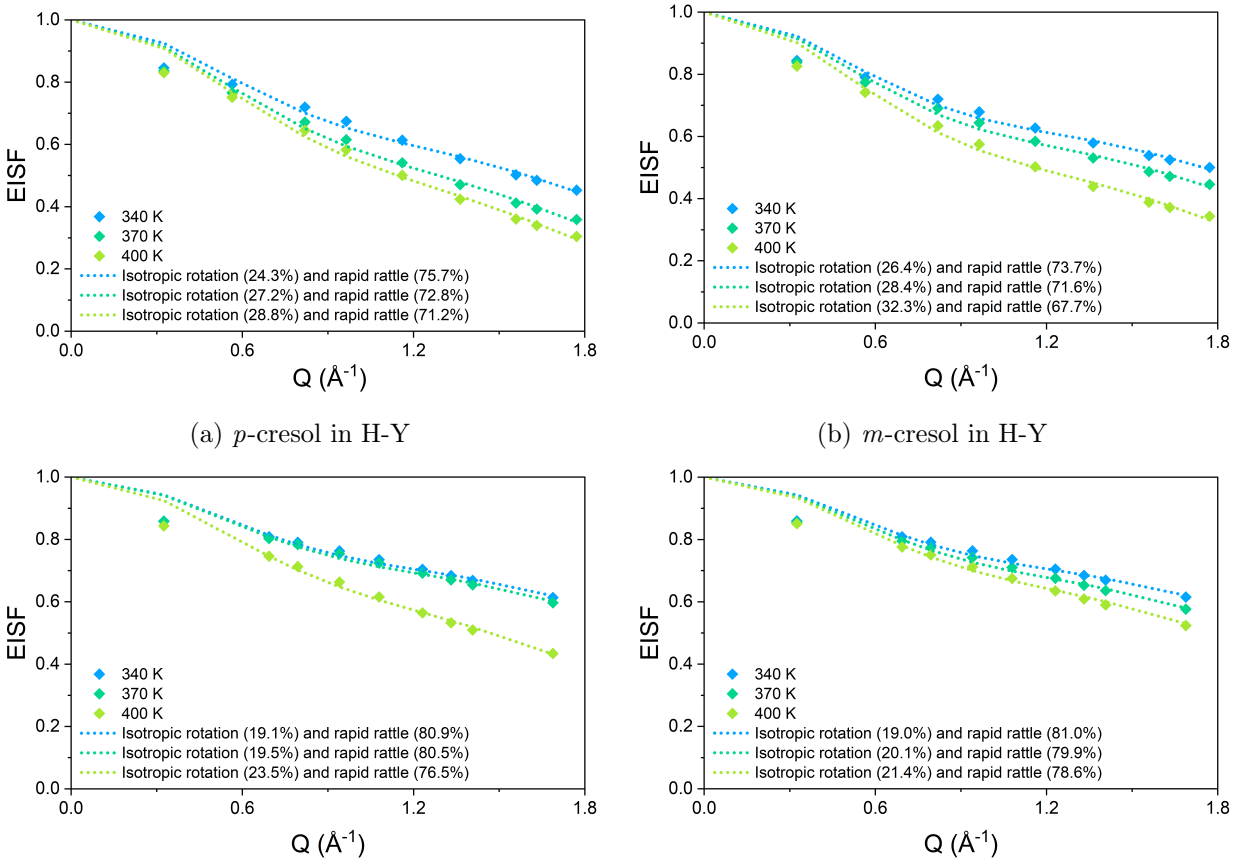

(a) *p*-cresol in H-Y

(b) *m*-cresol in H-Y

(c) *p*-cresol in H-Beta

(d) *m*-cresol in H-Beta

Figure S13: Simulated EISF of *m*- and *p*-cresol in H-Y and H-Beta from 340–400 K, fit by combined models of isotropic rotation and rapid rattling (isotropic rotation with varying radii). Percentages of each individual model contributing to the combined model are shown in brackets.

The HWHM data calculated from the MD simulations at 370 K are shown in figure S14 showing the trends with sample type, and every sample from 340–400 K are displayed in figure S8, from which the rotational coefficients were calculated.

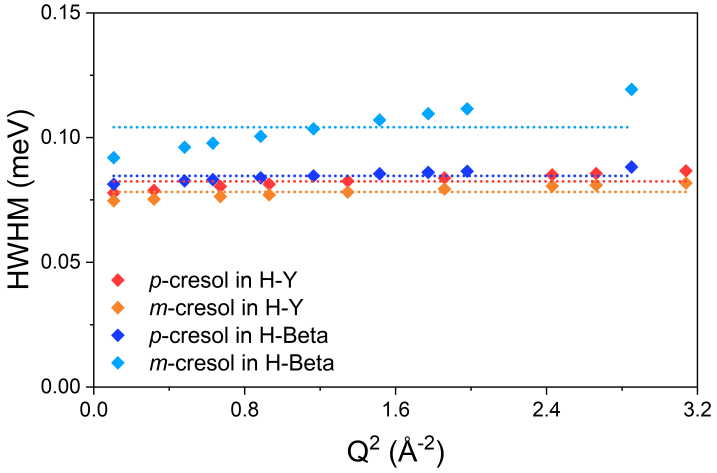

Figure S14: HWHM corresponding to Γ_1 calculated from MD simulations for *m*- and *p*-cresol in H-Y and H-Beta at 370 K, fit by models of rotation.

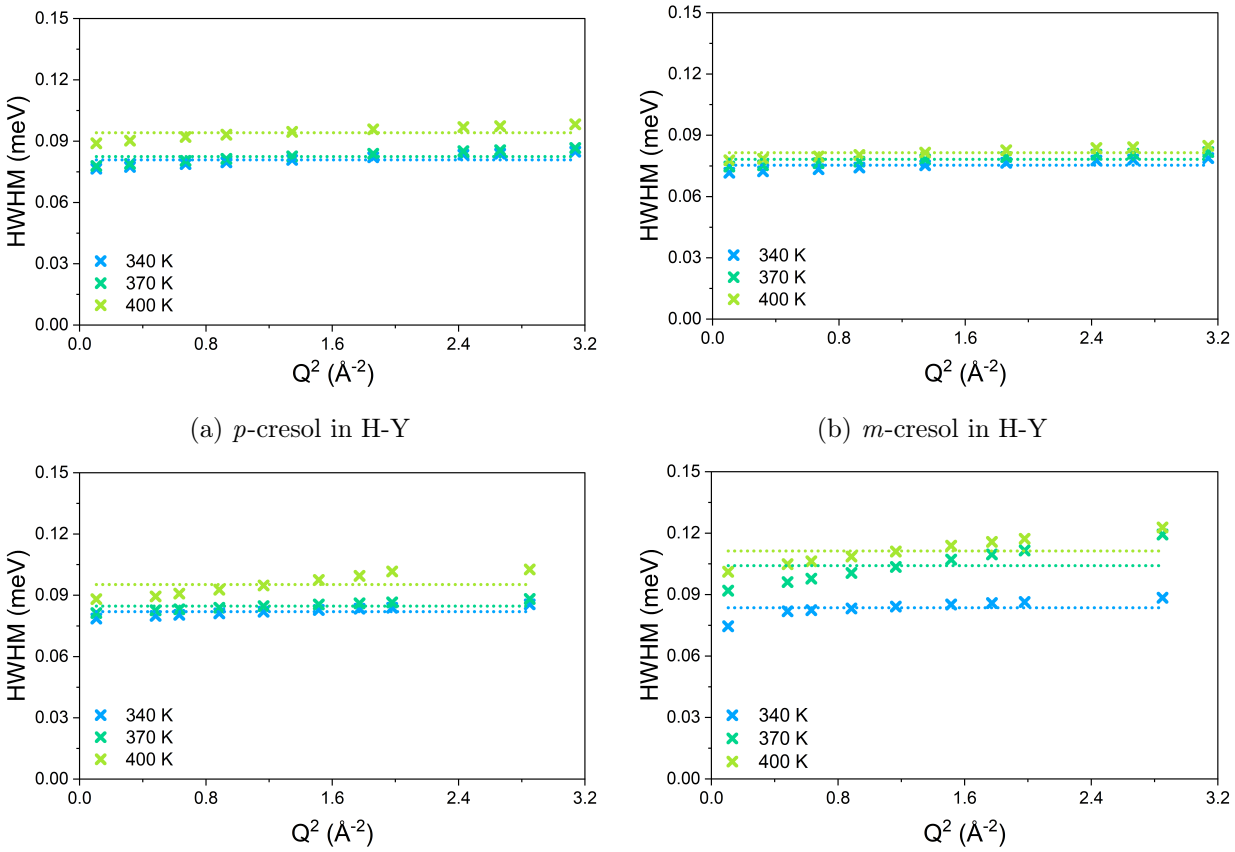

(a) *p*-cresol in H-Y

(b) *m*-cresol in H-Y

(c) *p*-cresol in H-Beta

(d) *m*-cresol in H-Beta

Figure S15: HWHM corresponding to Γ_1 calculated from MD simulations of *m*- and *p*-cresol in H-Y and H-Beta from 340–400 K, fit by models of rotation.

The rotational coefficients calculated from the MD simulations were used to calculate their respective activation energies via the Arrhenius plots shown in figure S16.

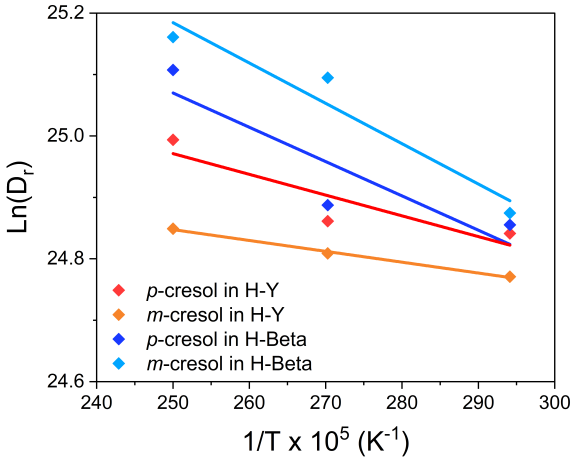

Figure S16: Arrhenius plots used to calculate the simulated E_a values for isotropic rotation.

S3.2 Bonding interactions

Intermolecular cresol-cresol H-bonding is shown by the RDF plots in figure S17.

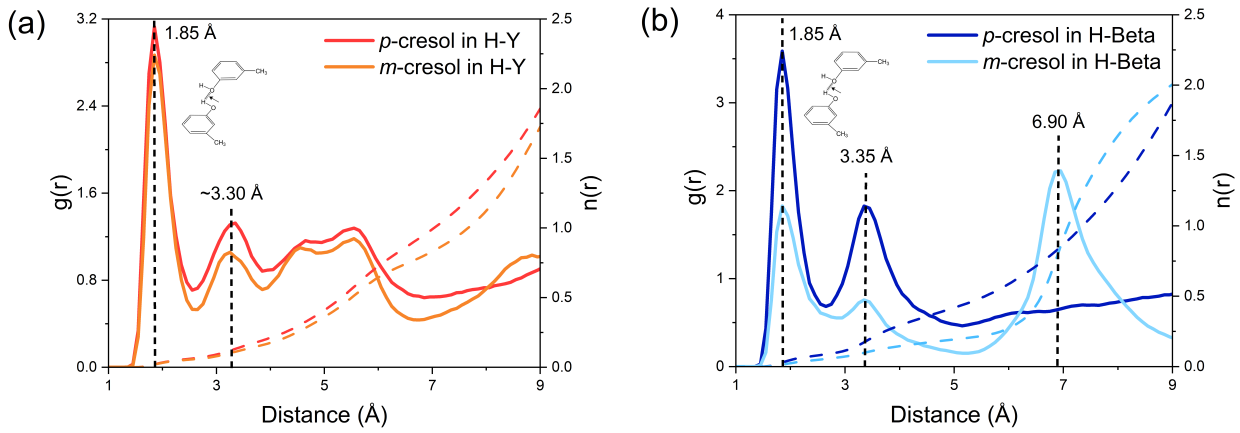

(a) (b)

Figure S17: RDFs (g(r)) between the cresol hydroxy group oxygen and hydrogen on different molecules and the associated coordination numbers (n(r)) of *p*- and *m*-cresol in (a) H-Y and (b) H-Beta at 370 K.

The presence of free cresol molecules is demonstrated by the prevalence of intermolecular cresol-cresol bonding through their hydroxyl groups in figure S17. Slightly more cresol-cresol interactions are present for the *p*-cresol isomers, however in both systems the number of cresols that are free to form H-bonds and also within hydrogen bonding distance of each other is small (average n(r) of 0.06 for cresol-cresol interactions). Intermolecular bonding occurs at an average distance of ∼1.9 Å, followed by a second shell occurring with lower frequency at ∼3.3 Å. These values are consistent with the hydrogen bonding distance and structure observed in simulations of liquid cresol[5]. The bonding distance in figure S17(b) at 6.90 Å corresponds to the distance between cresol molecules lined up on adjacent acid sites, though we note that this would likely not be reproduced by a more heterogeneous model of H-Beta, with differing aluminium distributions.

Shown in figure S18 is the radial distribution function (RDF) plot between the cresol oxygen and the BAS oxygen for cresols within H-Beta and their running integrals, calculated from the MD simulations. A distance of 3 Å is labelled for comparison with the cut-off distance applied in figures S19 and S20, for analysing the frequency of hydrogen bonding.

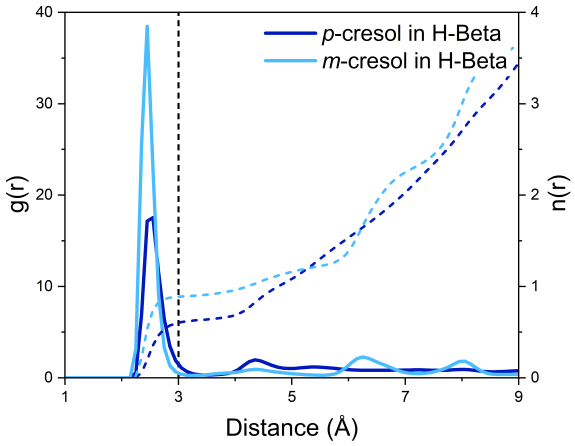

Figure S18: RDFs (g(r)) between the cresol oxygen and zeolite BAS oxygen and the associated coordination numbers (n(r)) of *p*- and *m*-cresol in H-Beta at 370 K.

VMD was used to calculate the number of hydrogen bonds at each timestep, where a hydrogen bond between a cresol hydroxyl group and zeolite BAS was defined as having an O-H—O angle of 180° ± θ, which was modelled as flexible in this instance by allowing θ to vary, to observe the effect of bonding angle on the frequency of adsorbate-zeolite H-bonds. The oxygen-to-oxygen cut-off distance was set to 3 Å, based on figure S18.

Shown in figure S19 is the number of hydrogen bonds per molecule against θ, from which figure S20 was created.

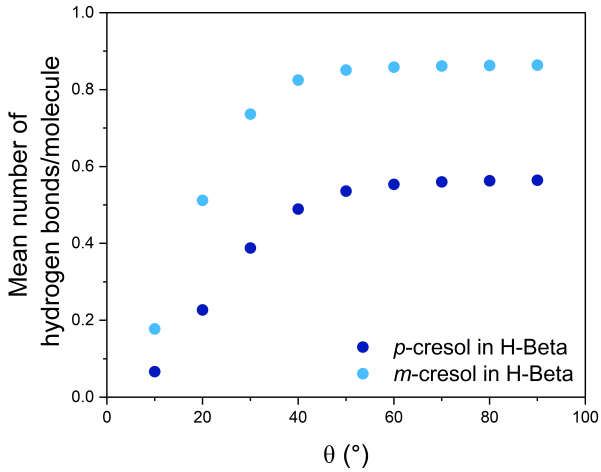

Figure S19: Frequency of hydrogen bonding per molecule as θ increases, deviating from a linear O_{cresol}–$HO_{zeolite}$ bonding angle, for *p*- and *m*-cresol in H-Beta at 370 K.

To calculate the normalised probability distribution of hydrogen bonds, shown in figure S20, the number of hydrogen bonds for ranges of θ values were divided by their respective integrals.

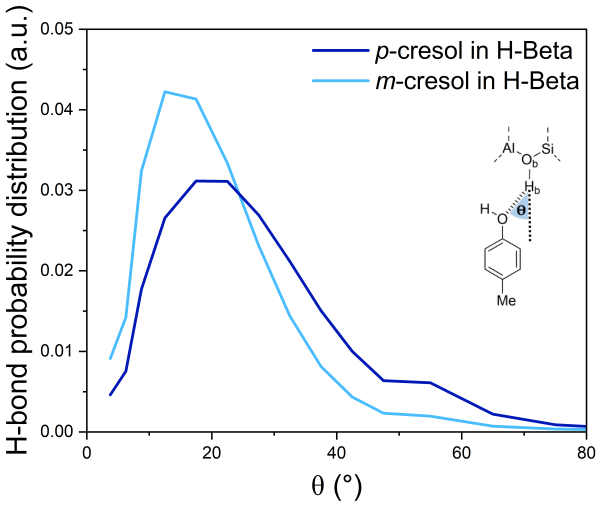

Figure S20: Normalised hydrogen bonding probability distribution against its bonding angle as it increases away from a linear O–H_b-O_b angle (θ), for *p*- and *m*-cresol in H-Beta at 370 K.

The average hydrogen bonding angle has a more narrow distribution of bonding angles around an optimal bonding arrangement for the *m*-cresol molecule in H-Beta compared to the *p*-cresol isomer, with their respective mean values of θ being approximately 15° and 20°. The *m*-isomer on average forms more linear and stronger hydrogen bonds, with 51% of molecules forming hydrogen bonds of 180° ± 20, as shown in figure S16, which must include molecules that are able to bond to BASs in the H-Beta channels. The hydrogen bonding angle distribution is much broader for *p*-cresol, and with averagely less linear bonding angles. It was found that a much smaller proportion (23%) of *p*-cresol molecules have θ values $\leq$20°, which could correspond to molecules present in the larger channel intersections where there is sufficient space for more linear bonding. For either isomer there is little probability of molecules being at an angle where θ>50° and still within a distance of <3 Å, as any bonds meeting this criteria are possibly not strong enough to be maintained, leaving the molecule free to undergo diffusion/rotation dynamics. Comparing the total number of hydrogen bonds over the total lengths of the simulations, *p*-cresol in H-Beta is less likely to H-bond to the acid sites compared to *m*-cresol, by a factor of ∼1.5, as observed in figure S16. The analysis suggests that *p*-cresol compared to *m*-cresol, on average, forms fewer and weaker interactions with the zeolite BASs when loaded into H-Beta. Potentially this is due to steric effects restricting the angle of bonding of the longer *p*-cresol molecule, rather than the slight electronic differences between the two molecules.

S3.3 Nanoscale diffusivity

The MSD plots calculated from the MD simulations at 370 K are shown in figure S21 showing the trends with sample type, and every sample from 340–400 K are displayed in figure S22, from which the diffusion coefficients were calculated.

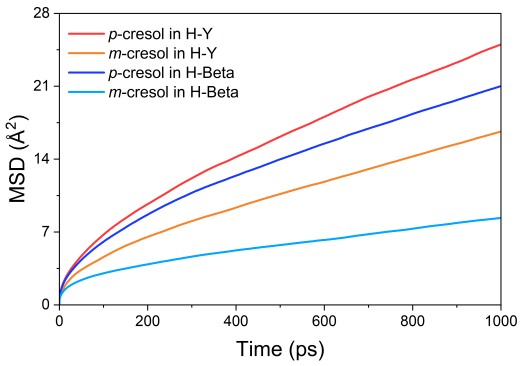

Figure S21: MSD plots of *p*- and *m*-cresol in H-Y and H-Beta at 370 K, averaged over 1 ns.

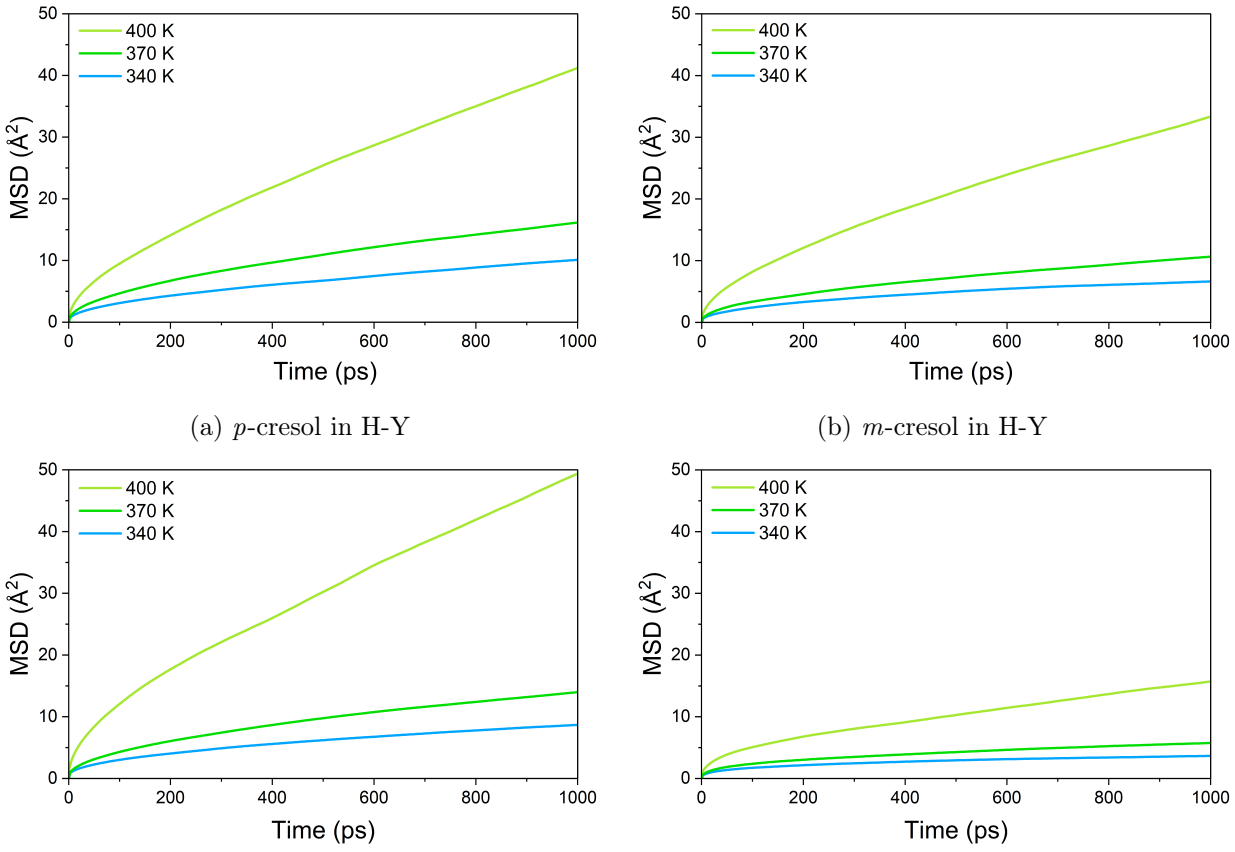

(a) *p*-cresol in H-Y

(b) *m*-cresol in H-Y

(c) *p*-cresol in H-Beta

(d) *m*-cresol in H-Beta

Figure S22: MSD plots of *p*- and *m*-cresol in H-Y and H-Beta from 340–400 K, averaged over 1 ns of MD simulations.

The D_s for translational diffusion obtained from the MSD plots (S22) were used to calculate their respective activation energies via the Arrhenius plots shown in figure S23.

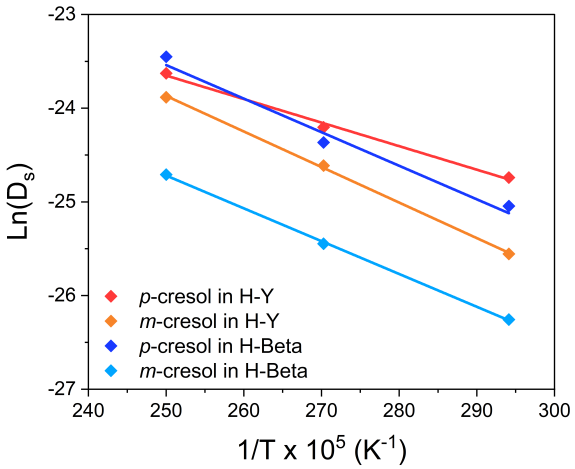

Figure S23: Arrhenius plots used to calculate the simulated E_a values for self-diffusion.

S3.4 Nanoscale diffusivity at catalytic temperatures

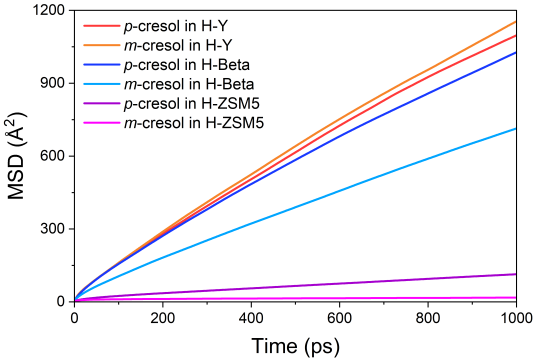

Figure S24: MSD plots of *p*- and *m*-cresol in H-Y, H-Beta and H-ZSM5 at 653 K, averaged over 1 ns.

References

[1] H. G. C. Baerlocher, L.B. McCusker, B. Marler, Database of disordered zeolite structures, http://www.iza-structure.org/databases/ (2023).

[2] F. Volino, A. Dianoux, Neutron incoherent scattering law for diffusion in a potential of spherical symmetry: general formalism and application to diffusion inside a sphere, Molecular Physics 41 (2) (1980) 271–279. doi:10.1080/00268978000102761.
URL `https://doi.org/10.1080/00268978000102761`

[3] V. F. Sears, Theory of cold neutron scattering by homonuclear diatomic liquids: I. free rotation, Canadian Journal of Physics 44 (6) (1966) 1279–1297. doi:10.1139/p66-108.
URL `https://doi.org/10.1139/p66-108`

[4] C. Hernandez-Tamargo, I. P. Silverwood, A. J. O'Malley, N. H. de Leeuw, Quasielastic neutron scattering and molecular dynamics simulation study on the molecular behaviour of catechol in zeolite beta, Topics in Catalysis 64 (9-12) (2020) 707–721. doi:10.1007/s11244-020-01400-1.
URL https://doi.org/10.1007/s11244-020-01400-1

[5] K. S. C. Morton, A. M. Elena, J. Armstrong, A. J. O'Malley, Experimental and modeling studies of local and nanoscale *para*-cresol behavior: A comparison of classical force fields, The Journal of Physical Chemistry A 127 (15) (2023) 3305–3316. doi:10.1021/acs.jpca.2c08022.
URL https://doi.org/10.1021/acs.jpca.2c08022